Letter

Direct observation of strong t_{2g}-e_g orbital hybridization and effects of f orbitals in a molecular analogue of chromium perovskite

Mian Wang, Chengzhi Li, Xiang-Guo Li,* and Yanglong Hou
School of Materials, Sun Yat-sen University, Shenzhen 518107, China

(Received 4 April 2024; revised 29 June 2024; accepted 16 July 2024; published 31 July 2024)

Chromium-based perovskites have drawn plenty of attention due to their intriguing magnetic properties and potential technique applications. While a complete understanding of the microscopic magnetic mechanisms underlying their macroscopic properties presents great challenges, especially when involving t_{2g}-e_g (t-e) hybridization and rare earth (RE) f orbitals. Here, with the recently discovered molecular analogue of perovskite $[Ce_2^{III}Ce^{IV}Cr_8^{III}O_8(O_2CPh)_{18}(HO_2CPh)]$, abbreviated as Ce_3Cr_8, we combine first-principles calculations and a superexchange model to successfully identify an anomalous ferromagnetism (FM)-dominated superexchange interaction between Cr ions originated from the t-e hybridization, which does not follow Goodenough-Kanamori rules. The great sensitivity of the t-e hybridization with respect to the angle of Cr-O-Cr can lead to a significant change in the magnetic interaction of Ce_3Cr_8 with the angle of Cr-O-Cr varying within only a few degrees, e.g., a ground-state transition from FM to antiferromagnetism. Additionally, the Ce f orbitals near the Fermi level can largely reduce this sensitivity by interacting with the Cr d orbitals via the virtual charge transfer process. Our results are strongly supported by an extended superexchange model developed with the inclusion of f orbitals within the t-e hybridization framework. These findings complete the theory of superexchange magnetism in chromium-based perovskites including RE f orbitals and in the meanwhile introduce a new avenue for fine-tuning the magnetic characteristics via modifying the transition metal d/RE f interactions at the nanoscale.

DOI: 10.1103/PhysRevB.110.L020409

Introduction. Magnetic perovskite materials continue to attract widespread attention in the scientific community due to their excellent and fascinating physical properties such as colossal magnetoresistance and multiferroicity [1–7]. In particular, the chromium-based $RECrO_3$ (RE = rare earths) compounds show a broad application in the fields of catalyst, thermistor, fuel cell, and nonvolatile memory devices because of their intriguing magnetic and ferroelectric properties [8]. However, understanding the underlying magnetic exchange mechanisms still presents great challenges due to their complexity. For example, a ferromagnetism (FM) from the t-e hybridization between Cr^{III} ions was reported previously in $RECrO_3$ [8–11]; however, the evidence is indirect and not adequate since the antiferromagnetic (AFM) superexchange interaction is still the main contribution to the exchange interactions of Cr^{III}-O-Cr^{III} with the bridging angle being much greater than 90° in bulk $RECrO_3$, according to the Goodenough-Kanamori (GK) rule [12–14]. The dominance of the FM superexchange interaction in such geometry, that is, the direct evidence of the existence of t-e hybridization-induced FM interaction, has never been achieved, not to mention the quantitative analysis of this FM interaction.

The recently synthesized molecular analogue of the perovskite repeating unit $[Ce_2^{III}Ce^{IV}Mn_8^{III}O_8(O_2CPh)_{18}(HO_2CPh)$, abbreviated as Ce_3Mn_8], which manifests rich and complex physics with a variety of magnetic interactions involving f electrons [15], provides a new platform for the underlying exchange mechanism investigations. Introducing an extra d_σ electron by substituting Mn^{III} with Fe^{III} can result in more pronounced asymmetric behavior in the FM interaction involving transition metal (TM) $3d$ and RE $4f$ orbitals [16]. Cr^{III}, on the other hand, without occupied d_σ orbitals can potentially exhibit more novel physics. For example, the more distorted molecular geometry compared to its bulk counterpart may present a different degree or form of t-e hybridization. The RE f orbitals can also potentially have significant effects on the t-e hybridization. In addition, the nanoscale size of the molecule enables the fine-tuning of its properties by chemical doping or external manipulation, which is intrinsically different from its corresponding bulk perovskite. Consequently, it is desirable to study these fundamental physics related to the magnetic exchange mechanisms in the molecular form of RE-Cr systems.

In this Letter, we theoretically explore the complex magnetism in Ce_3Cr_8, a molecular analogue of the perovskite repeating units, by replacing Mn ions with Cr ions in Ce_3Mn_8 [15,17], with the main focus on the t-e hybridization and the effects of f orbitals using the first-principles method. Interestingly, our calculations show that FM exchange coupling between Cr ions via t-e hybridization is the dominant interaction in Ce_3Cr_8, leading to a FM ground state, distinct from its bulk $RECrO_3$ crystal in which AFM interaction is still the leading interaction. The calculated exchange strengths at various Coulomb energies and Cr-O-Cr bond angles quantitatively agree with a simple model derived from orbital overlap

*Contact author: lixguo@mail.sysu.edu.cn

integration, further confirming the FM nature of *t*-*e* hybridization. More importantly, the Ce^{IV} *f* orbitals around the Fermi level can significantly change the sensitivity of strain-induced exchange coupling changes through the virtual charge transfer between Ce 4*f* orbitals and Cr 3*d* orbitals, different from the direct FM contribution from *f* orbitals in Ce_3Mn_8 [15] and Ce_3Fe_8 [16]. Our results add extra content for the fundamental superexchange coupling physics by directly demonstrating the dominant FM interaction in TM-O-TM with a bonding angle much greater than 90°. The effects of *f* orbitals on such an exchange mechanism can provide another dimension to modify and control the magnetic behavior in magnetic molecular-based devices.

Method. Our first-principles calculations were carried out within the framework of the Kohn-Sham density functional theory (DFT) [18] with the generalized gradient corrected Perdew-Burke-Ernzerhof exchange-correlation function [19] using the Vienna Ab-initio Simulation Package (VASP) code [20,21]. The electron-ion interaction was described using projector augmented-wave potentials [22,23]. The energy cutoff for plane-wave basis expansion was set to 500 eV. The thresholds for self-consistency and structure optimization were set to 10^{-5} eV and 0.01 eV/Å, respectively. The molecule was put into a large periodic supercell of 28 Å × 22 Å × 24 Å to make sure the distance between the molecule and its repeating image was larger than 10 Å. Because of the strong localization of RE *f* orbitals and Cr *d* orbitals, the generalized gradiant approximation (GGA)+*U* method was applied with $U = 2.0$ eV [15,16,24] for the RE *f* orbitals, in line with our previous work showing consistent results with experiment [15]. For Cr *d* orbitals, we chose *U* values ranging from 1.5 to 5.0 eV to verify our findings. We used the results with *U* equaling 3.0 eV for ease of description. A negative homogeneous background charge was added in $[La_3Cr_8]^{-1}$ calculations to keep the valence state of Cr as +3. All other calculation details for $[La_3Cr_8]^{-1}$ were the same as those for Ce_3Cr_8. The WANNIER90 package [25] was applied to calculate Wannier functions. The spin-orbital coupling was switched off due to its negligible effects on the exchange coupling in 3*d* and 4*f* compounds [16,26,27]. We changed the bond angle of Cr-O-Cr by moving the O atom along the *c* axis and fixing all other atoms. The bond angle of Cr-O-Cr could change around 2° with the O atom moving approximately 0.03 Å.

Results. The initial structure of the Ce_3Cr_8 molecule is obtained by substituting Cr ions for Mn ions in the recently reported Ce_3Mn_8 molecule [15]. Analogous to $Ce_3Mn_8^{III}$, the $Ce_3Cr_8^{III}$ molecule has a striking structural similarity to the repeating unit of perovskite, which resembles a repeating unit of ABO_3 cubic with distortions and plus two *A* ions, as shown in Figs. 1(a) and 1(b). The core of $Ce_3Cr_8^{III}$ includes eight Cr sites and three Ce sites. Three Ce ions are arranged in a line as shown in Fig. 1(b). The central Ce ion has an oxidation state of +4 and is eight-coordinated, while the other two Ce ions have an oxidation state of +3 and are nine-coordinated. The eight Cr^{III} ions in $Ce_3Cr_8^{III}$ can be divided into two groups, each group has four Cr^{III} ions, which are separated by the Ce line, denoted as the top group (Cr1, Cr2, Cr3, Cr4) and the bottom group (Cr5, Cr6, Cr7, Cr8).

We perform the subsequent electronic structure calculations after a full geometry optimization. We mainly focus on

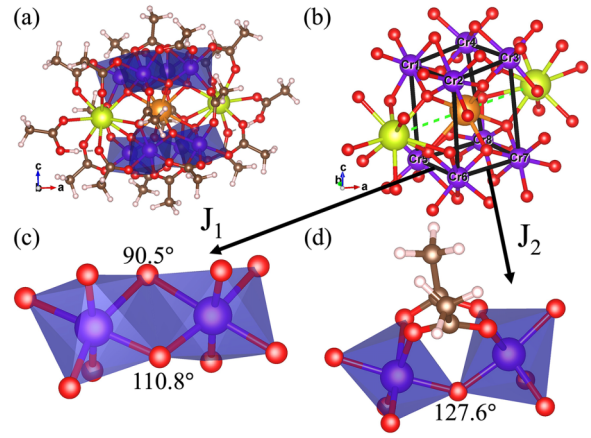

FIG. 1. The optimized molecular structure of Ce_3Cr_8. (a) The complete molecular structure of Ce_3Cr_8 with $–CH_3$ as the ligand group. The CrO_6 octahedra are shaded in blue. Color scheme: Ce^{IV}, orange; Ce^{III}, green; Cr^{III}, purple; and O, red. (b) The partial Ce_3Cr_8 central fragment without ligands, showing only the Ce-O and Cr-O bonds. The Ce line is denoted by a green dotted line. The Cr curb is labeled by black lines. The enlarged structures of (c) path J_1 and (d) path J_2. The average degrees of ∠Cr-O-Cr are labeled.

the nearest-neighbor (NN) exchange couplings of the Cr ions along the paths involving Cr-O-Cr geometries, including J_1 perpendicular to the Ce line [see Fig. 1(c)] and J_2 parallel with the Ce line [see Fig. 1(d)]. In the neighboring CrO_6 of path J_1, the two Cr-O octahedras are edge sharing with two bridging oxygen atoms with Cr-O-Cr bonding angles of 110.8° and 90.5°, respectively [see Fig. 1(c)]; the neighboring CrO_6 within the path J_2 shares one corner with one bridging oxygen atom with Cr-O-Cr bonding angles of 127.6°, and two carboxylate groups connect the two Cr ions within the neighboring CrO_6 octahedras [see Fig. 1(d)].

The perovskites have four known common types of spin-ordering configurations: FM, A-AFM, C-AFM, and G-AFM [28], while the Ce_3Cr_8 molecule has low symmetry with three inequivalent interaction planes or axes along different orientations, leading to three distinct A-AFM states and three different C-AFM states. Thus, there are eight highly symmetrical magnetic configurations (plus one G-AFM state and one FM state) in Ce_3Cr_8, illustrated in Fig. S1 of the Supplemental Material [29]. Our results, obtained by performing DFT + *U* calculations for all eight magnetic configurations, show that the FM state is the ground state of the Ce_3Cr_8 molecule. The calculated total energies of these eight magnetic configurations are listed in Table S1 of the Supplemental Material [29]. The eight Cr ions in Ce_3Cr_8 have a 2.8-μ_B magnetic moment for each Cr, which indicates an oxidation state of +3 [31]. The two Ce^{III} ions outside the Cr curb have magnetic moments of 1 μ_B for each, which is included in the core region of the charge density, and the central Ce^{IV} has small magnetic moments (less than 0.1 μ_B).

To reveal the underlying magnetic properties of Ce_3Cr_8, the Cr-Cr exchange coupling parameters (*J*) are estimated by a multispin Heisenberg model [32–36] with total energies of different magnetic states (see Table S1 of the Supplemental Material [29] for all energies we calculated in this work under different conditions). The spin Hamiltonian is

TABLE I. The exchange coupling parameters (J) in meV of Ce_3Cr_8 and $[La_3Cr_8]^{-1}$ for different distorted structures. The degree of the ∠Cr-O-Cr in the path of J_2 is shown in parentheses in the first column. The differences of the parameters in $[La_3Cr_8]^{-1}$ with respect to those in Ce_3Cr_8 are shown in parentheses in the last column.

J path	Ce_3Cr_8	$[La_3Cr_8]^{-1}$
J_1(relaxed structure)	1.09	1.54 (+0.45)
J_2(relaxed structure)	2.17	2.53 (+0.36)
J_2(∠Cr-O-Cr = 125°)	3.96	5.17 (+1.21)
J_2(∠Cr-O-Cr = 127°)	3.55	4.13 (+0.58)
J_2(∠Cr-O-Cr = 129°)	2.90	2.75 (−0.15)
J_2(∠Cr-O-Cr = 131°)	1.99	1.02 (−0.97)
J_2(∠Cr-O-Cr = 133°)	0.81	−1.09 (−1.90)

defined as

$$\hat{H} = -\sum_{i<j} J_{ij}\vec{S}_i \cdot \vec{S}_j, \tag{1}$$

where J_{ij} are magnetic coupling parameters between the Cr ions at sites i and j; $\vec{S}_i$ and $\vec{S}_j$ are the spin vectors of Cr ions at sites i and j, respectively. The exchange coupling constants are calculated within the broken-symmetry density functional theory framework using the spin-projected approach [37]. The total spin of S is $\frac{3}{2}$ for each Cr ion according to the Hund's rule. The spins of Ce^{III} are not included in the Heisenberg model due to their weak exchange couplings in the mixed $3d$-$4f$ molecules as demonstrated by previous experimental results [15,38]. Our total energy results indicate that two spin-coupling paths, J_1 to J_2 (see Fig. 1), exhibit significant contributions to the total energy. Other coupling paths with relative longer distances between Cr ions, e.g., the diagonal direction of faces (J_3) and the path connecting the top and bottom Cr groups (J_4) (see Fig. S1 of the Supplemental Material [29]), are much smaller compared to J_1 and J_2 (J_3 = +0.25 meV, J_4 = +0.07 meV, see Table S2 of the Supplemental Material [29]). The calculated coupling strengths (see Table I) are J_1 = +1.09 meV and J_2 = +2.07 meV (positive for FM, negative for AFM). The strong FM interactions of J_1 and J_2 result in the FM ground state.

The FM interactions of J_1, J_3, and J_4 are understandable. According to GK rules, the superexchange Cr-O-Cr with a bond angle of 90.5° in path J_1 can provide FM interaction. Additionally, based on our previous work [15], the direct FM exchange through Cr^{III}-Ce^{IV}-Cr^{III} should still exist but be much weaker since Cr^{III} does not contain d_σ electrons, which can result in a weak FM coupling in J_3 and J_4. The dominant FM nature of J_2 is unexpected after analyzing the superexchange mechanisms. For example, in the J_2 exchange coupling pathway, the superexchange through Cr-O-Cr (∠Cr-O-Cr = 127.6°) should contribute AFM interactions according to the GK rules [8,15]. The reported FM contribution from the the t_{2g}-e_g (t-e) hybridization on the Cr^{III}-O-Cr^{III} couplings via the virtual charge transfer (VCT) of t_{2g}^3-O-e_g^0 is much weaker compared to the AFM interaction in bulk $RECrO_3$ crystal [9]. As such, J_2 should exhibit an AFM nature, or at least not a FM-dominated nature. We attribute this strong FM nature to the more distorted molecular structure compared to its bulk crystal, which can induce much larger tilting in the Cr-O octahedron and lead to much stronger t-e hybridization. This assessment is further confirmed by quantitatively evaluating the competing mechanisms between AFM and FM in J_2, as shown next.

In the framework of t-e hybridization, the superexchange interactions of Cr^{III} ions include two parts: the superexchange interactions over the half-filled π bond t_{2g}^3-O-t_{2g}^3, which is AFM according to the GK rules; the interaction between the half-filled π bond and the empty σ bond, i.e., t_{2g}^3-O-e_g^0, due to the introduction of a VCT to the empty σ bond from t-e hybridization, which shows the FM coupling (see Fig. S2 of the Supplemental Material [29] for the corresponding schematic hybridization diagram). The sum of these two parts gives the total interaction J in the J_2 path, as shown below [9],

$$J = J_\sigma - J_\pi, \tag{2}$$

where J_π expresses the AFM interaction via the VCT of t_{2g}^3-O-t_{2g}^3 and the J_σ denotes FM interaction via the VCT of t_{2g}^3-O-e_g^0 due to t-e hybridization. They can be further expressed in an analytical form by considering all possible orbital overlap integration between O and Cr [9] (see Sec. I A of the Supplemental Material [29] for detailed derivation), as shown below,

$$J = J_0[\eta(d_\sigma)^2 - (d_\pi)^2], \tag{3}$$

$$J_0 = \frac{(V_{pd\pi})^2}{U + \triangle_{ex}}, \tag{4}$$

$$\eta = \frac{(V_{pd\sigma})^2}{(V_{pd\pi})^2}\frac{U + \triangle_{ex}}{U + \triangle_c}, \tag{5}$$

$$d_\sigma = \left[\cos\left(\frac{W}{2}\right) + \sin\left(\frac{W}{2}\right)\right]\left\{\sqrt{3}\cos\left(\frac{W}{2}\right)\sin\left(\frac{W}{2}\right) + \frac{\sqrt{3}}{2}\left[\cos^2\left(\frac{W}{2}\right) - \sin^2\left(\frac{W}{2}\right)\right] - \frac{1}{2}\right\}, \tag{6}$$

$$d_\pi = 2\left[\sin\left(\frac{W}{2}\right) + \cos\left(\frac{W}{2}\right)\right] - 4\sin\left(\frac{W}{2}\right)\cos^2\left(\frac{W}{2}\right), \tag{7}$$

where J_0 is a prefactor depending on the orbital overlap integral $V_{pd\pi}$, the on-site Coulomb U, and the exchange splitting $\triangle_{ex}$; and η is a dimensionless parameter defined as the multiplication of two ratios, the orbital overlap integral ratio $\left(\frac{(V_{pd\sigma})^2}{(V_{pd\pi})^2}\right)$ and the energy ratio $\left(\frac{U+\triangle_{ex}}{U+\triangle_c}\right)$. $\triangle_c$ is the crystal-field splitting; d_π and d_σ are parameters evolving with the bridging angle of ∠Cr-O-Cr (W) [8,9,39]. In order to quantitatively determine the origin of FM in Ce_3Cr_8, we calculated a series of J_2 values (see Table I) by computing the total energies of the eight magnetic states in different cases (see Table S1 of the Supplemental Material [29] for the energies of each case), including (i) the Ce_3Cr_8 molecule with different angles of ∠Cr-O-Cr in J_2 (125°, 127°, 129°, 131°, 133°); and (ii) the $[La_3Cr_8]^{-1}$ molecule with different angles of ∠Cr-O-Cr in J_2 (125°, 127°, 129°, 131°, 133°). The $[La_3Cr_8]^{-1}$ molecule is obtained by replacing the Ce ions with La ions and adding

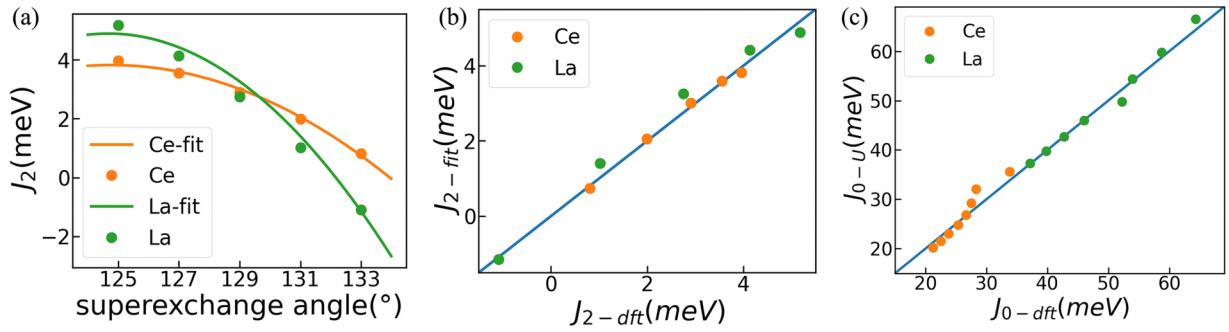

FIG. 2. Plot of superexchange strength from DFT-calculated and model-fitted values in Ce_3Cr_8 and $[La_3Cr_8]^{-1}$. (a) J_2 from DFT versus the superexchange angle Cr-O-Cr. (b) J_2 from model-fitted values according to Eq. (3) ($J_2 - fit$) versus DFT calculated values ($J_2 - dft$). (c) J_0 calculated from Eq. (4) ($J_0 - U$) versus fitted from DFT results according to Eq. (3) ($J_0 - dft$).

an additional electron to keep the valence state of Cr ions unchanged. The choice of the $[La_3Cr_8]^{-1}$ molecule was inspired by our previous work [15,16] showing that the unoccupied Ce^{IV} f orbital can enhance the FM interaction between transition metals after comparing the exchange coupling strengths between $[Ce_3TM_8]$ and $[La_3TM_8]^{-1}$.

With the data of the angle-dependent J_2 in Table I, we then fit Eq. (3) by setting J_2 [J in Eq. (3)] as the y values, angle W as the x values, and J_0 and η as the fitting parameters. An excellent fit was obtained, as shown with the fitted curves as well as the corresponding parity plot [see Figs. 2(a) and 2(b)]. This clearly indicates the validity of Eq. (3) in describing the exchange mechanisms in Ce_3Cr_8 and $[La_3Cr_8]^{-1}$. The fitted values for parameters J_0 and η are 26.63 meV and 1.86, respectively, for Ce_3Cr_8 and 52.22 meV, and 1.81 for $[La_3Cr_8]^{-1}$. The J_0 for Ce_3Cr_8 is about half of that in $[La_3Cr_8]^{-1}$, while η is almost unchanged, whose value is also reasonable [9]. The value of J_0 determines the sensitivity of the change of J_2 with respect to the superexchange angle of TM-O-TM. With the increase of the TM-O-TM angle, the exchange coupling can eventually turn to AFM dominated, e.g., the studied superexchange J_2 (see Table I). Thus, the exchange coupling in Ce_3Cr_8 does not always show more FM nature than that in $[La_3Cr_8]^{-1}$, which is different from Ce_3Mn_8 [15] or Ce_3Fe_8 [16]. The validity of Eq. (4) is further demonstrated with the following steps.

(i) Select a series of U values (1.5, 2.0, 2.5, 3.0, 3.5, 4.0, 4.5, and 5.0 eV). At each U value, calculate angle-dependent J_2 values and fit Eq. (3) to obtain the fitted J_0 for each U value (see Tables S1, S3, and S4 of the Supplemental Material [29] for the detailed calculation data).

(ii) Estimate $\triangle_{ex}$ by constructing the maximally localized Wannier functions (MLWFs) based on the ferromagnetic electronic structure [40]. Our estimated values of $\triangle_{ex}$ are 4.3 and 4.2 eV for Ce_3Cr_8 and $[La_3Cr_8]^{-1}$, respectively, when $U =$ 3.0 eV. The change of $\triangle_{ex}$ is about one-fifth of the change of U values, e.g., $\triangle_{ex1} - \triangle_{ex2} = 1/5(U_1 - U_2)$.

(iii) Fit Eq. (4) by setting J_0 obtained from step 1 as the y values, U as the x values, and $V_{pd\pi}$ as the fitting parameters.

The corresponding parity plot with a unity slope is shown in Fig. 2(c) (see Fig. S3 of the Supplemental Material [29] for the fitted curves), which indicates the effectiveness of Eq. (4) in describing the U dependence of J_0. Overall, the superexchange model within the framework of t-e hybridization can correctly describe our DFT-calculated results in RE_3Cr_8, confirming that the extraordinary FM-dominated exchange coupling in the molecule is originated from the t-e hybridization, which is distinct with its bulk crystal due to the much larger distortion with even smaller TM-O-TM angles in the molecules.

To go deeper, we can observe that J_0 in Ce_3Cr_8 (26.63 meV) is around half of that in $[La_3Cr_8]^{-1}$ (52.22 meV), which is responsible for the much less sensitivity of J_2 with respect to the TM-O-TM angles in Ce_3Cr_8 [orange curve in Fig. 2(a)] compared to that in $[La_3Cr_8]^{-1}$ [green curve in Fig. 2(a)]. After analyzing the differences between Ce_3Cr_8 and $[La_3Cr_8]^{-1}$, we reasonably attribute the reason to the effect of the f orbitals. The projected density of states (PDOS) plots [see Figs. 3(a) and 3(b)] for FM states of both Ce_3Cr_8 and $[La_3Cr_8]^{-1}$ show that Ce f orbitals are much closer to the Fermi level compared to the La f orbitals. A higher degree of hybridization between Ce $4f$ orbitals and O $2p$ orbitals is also observed in Ce_3Cr_8; e.g., the PDOS of Ce $4f$ orbitals and O $2p$ orbitals have overlap peaks in Ce_3Cr_8, which is U independent [see Figs. 3(c) and 3(d) and Fig. S6 of the Supplemental Material [29] for the PDOS plots of other U values of Ce $4f$ orbitals and La $4f$ orbitals). The above evidence indicates that the VCT can happen in Ce-O but not in La-O. In addition, the fitted parameters $V_{pd\pi}$ in Eq. (4) are 0.42 and 0.60 eV for Ce_3Cr_8 and $[La_3Cr_8]^{-1}$, respectively. However, the similar hopping terms calculated from MLWFs (see Table S5 of the Supplemental Material [29]) and the same form of overlap integral in the Slater's approach [39] indicate that the orbital overlap integrals $V_{pd\pi}$ should be close to each other in the two systems. This discrepancy reminds us that a correction should be applied to the t-e hybridization framework to include the effects of f orbitals.

To include the f orbitals in the process of VCT, we extend the t-e hybridization framework according to the superexchange model [12–14,39,41](see Sec. I B of the Supplemental Material [29] for detailed analysis), as shown below,

$$J = J_d + J_f, \tag{8}$$

$$J_d = \frac{(b_{pd\sigma})^2}{U + \triangle_c} - \frac{(b_{pd\pi})^2}{U + \triangle_{ex}}, \tag{9}$$

$$J_f = 0.5\left[\frac{(b_{pd\pi})^2}{U + \triangle_{ex}} - \frac{(b_{pd\sigma})^2}{U + \triangle_c}\right] - \frac{(b_{pf\sigma})^2}{U + \triangle_f} + \frac{(b_{pf\pi})^2}{U + \triangle_f}, \tag{10}$$

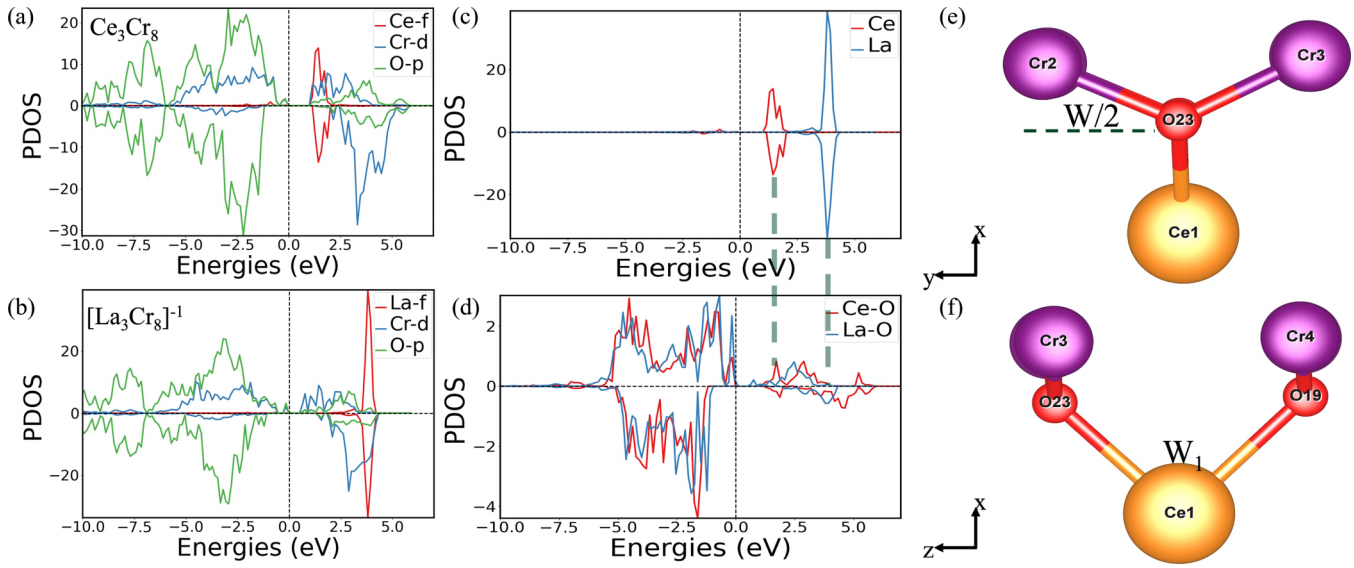

FIG. 3. The projected density of states (PDOS) for (a) the FM state (ground state) of Ce_3Fe_8 and (b) $[La_3Fe_8]^{-1}$, (c) Ce f orbitals and La f orbitals in Ce_3Cr_8 and $[La_3Cr_8]^{-1}$, and (d) O p orbitals along path J_2 in Ce_3Cr_8 and $[La_3Cr_8]^{-1}$. (e), (f) Schematic diagram of atomic structures along path J_2.

$$b_{pd} = d_{pd}V_{pd}, \quad b_{pf} = d_{pf}V_{pf} \tag{11}$$

$$J^{\mathrm{Ce}} = J_d + J_f = 0.5\left[\frac{\left(b^{\mathrm{Ce}}_{pd\sigma}\right)^2}{U+\triangle^{Ce}_{c}} - \frac{\left(b^{\mathrm{Ce}}_{pd\pi}\right)^2}{U+\triangle^{Ce}_{ex}}\right], \tag{12}$$

$$J^{\mathrm{La}} = J_d = \frac{\left(b^{La}_{pd\sigma}\right)^2}{U+\triangle^{\mathrm{La}}_{c}} - \frac{\left(b^{\mathrm{La}}_{pd\pi}\right)^2}{U+\triangle^{\mathrm{La}}_{ex}}, \tag{13}$$

$$J^{\mathrm{La}}_0 = \frac{\left(V^{\mathrm{La}}_{pd\pi}\right)^2}{U+\triangle^{\mathrm{La}}_{ex}}, \quad J^{\mathrm{Ce}}_0 = \frac{0.5\left(V^{\mathrm{Ce}}_{pd\pi}\right)^2}{U+\triangle^{\mathrm{Ce}}_{ex}}, \tag{14}$$

where J_d and J_f are the exchange coupling contributions from d orbitals and f orbitals, respectively. J^{Ce} and J^{La} are the exchange couplings in Ce_3Cr_8 and $[La_3Cr_8]^{-1}$, respectively. The different b variables are transfer integrals of corresponding orbitals (see Sec. IB of the Supplemental Material [29] for the complete formula). Equation (9) is the same as Eq. (3) after absorbing the dimensionless parameters d to the transfer integrals b, as shown in Eq. (11). J^{La}_0 (J^{Ce}_0) connects to J^{La} (J^{Ce}) through Eq. (3) with J^{La}_0 (J^{Ce}_0) and J^{La} (J^{Ce}) corresponding to J_0 and J in Eq. (3), respectively. For J_f in Eq. (10), the Ce-O bonds are approximately perpendicular to the J_2 path (the degree of ∠Cr-O-Ce is close to 90°) [see Figs. 3(e) and 3(f)], and thus the symmetry in the Ce-O-Cr bonds is opposite to that in the Cr-O-Cr bonds; that is, σ and π in Cr-O-Cr should be π and σ in Cr-O-Ce. To keep consistent notation of σ and π, an opposite sign of $\frac{(b_{pd\pi})^2}{U+\triangle ex}$ and $\frac{(b_{pd\sigma})^2}{U+\triangle c}$ is assigned in J_f in Eq. (10) compared to J_d in Eq. (9) [14]. The Cr-O-Cr path has two O^{2-}-Cr^{3+} exchange coupling interactions, while the Cr-O-Ce path only has one O^{2-}-Cr^{3+} exchange coupling according to Anderson's mechanism [41]. This leads to the prefactor of pd superexchange coupling in J_f being half of that in J_d. The b_{pf} contributions from the VCT to unoccupied $4f$ orbitals in $[La_3Cr_8]^{-1}$ can be ignored due to the negligible exchange interaction from the La f orbitals, as discussed in the previous paragraphs. However, even in Ce_3Cr_8, the b_{pf} is still an order of magnitude smaller than b_{pd} (see Sec. I B and Table S6 of the Supplemental Material [29]). Therefore, J_0 in Ce_3Cr_8 and $[La_3Cr_8]^{-1}$ can be finally expressed in the form of Eq. (14), which clearly indicates that J_0 in Ce_3Cr_8 (26.63 meV) is about half of that in $[La_3Cr_8]^{-1}$ (52.22 meV) after considering the effects of f orbitals. Noting that the $\frac{(V_{pd\pi})^2}{U+\triangle_{ex}}$ ratios in Ce_3Cr_8 and $[La_3Cr_8]^{-1}$ are approximately equal to each other.

Discussion. We have theoretically investigated the atomic structure and the electronic and magnetic properties of the molecule analogue of perovskite chromites, abbreviated as Ce_3Cr_8, using the first-principles method. In particular, we found an unexpected dominate FM interaction in magnetic coupling between two NN Cr sites with the angle Cr-O-Cr much greater than 90°, distinct from the bulk perovskite chromites [8,9]. The magnetic coupling between Cr ions evolving with the degree of ∠Cr-O-Cr follows the t-e hybridization theory, confirming that the dominated FM nature is originated from t-e hybridization. In particular, due to the great sensitivity of t-e hybridization with respect to the superexchange angle Cr-O-Cr, little molecular structure change can induce significant difference in the magnetic exchange coupling strength with the ground state evolving a transition from FM to AFM. This structure-dependent magnetic interaction mechanism can be applied to develop multifunctional molecule-based magnetic devices.

The effects of the RE f orbitals to the exchange interaction of TM ions was initially pointed out in Ce_3Mn_8 by contributing a direct FM interaction [15], which was also confirmed in Ce_3Fe_8 [16]. Our calculation results in Ce_3Cr_8 also indicate that the Ce f orbitals can have effects on the superexchange interaction between TM ions but with a different mechanism from the previous works. In Fig. 2(c), we can see that Ce f orbitals can significantly change the sensitivity of J_2 with respect to the molecular structural change, not just contributing

FM or AFM interaction. All these studies on the analysis of the effects of f orbitals show that only the orbitals near the Fermi level can have sizable contributions to the superexchange interaction. Hence the effects of f orbitals on the t-e hybridization are closely related to the energy level position of the orbitals, which can be modulated by the type of cations and TM elements, as well as the molecular geometry. For example, charging the molecule can significantly change the molecular geometries and energy levels of the orbitals [17,42] and thus, in turn, modify the magnetic interactions within the molecules.

Conclusion. In conclusion, our investigation of the Ce_3Cr_8 magnetic molecule elaborates the complex magnetism involving both t-e hybridization and RE f orbitals at the nanoscale. The superexchange via the Cr d orbitals and O p orbitals can provide a dominate FM interaction for both J_1 and J_2 through strong t-e hybridization induced by the structural distortion. The superexchange interaction involving the t-e hybridization is very sensitive to the molecular structure; e.g., the ground state can undergo a FM to AFM transition upon the structural change, which can be further modulated by the RE f orbitals. In particular, the inclusion of Ce f orbitals can decrease the sensitivity of the change of the magnetic coupling with respect to the molecular structural changes. Our theoretical work complements the theory of superexchange magnetism involving t-e hybridization and adds another dimension to fine-tune the magnetic properties of nanoscale molecules through TM d/RE f interactions.

Acknowledgments. The authors would like to acknowledge financial support from the Hundreds of Talents Program of Sun Yat-sen University. The authors also acknowledge the use of computing resources from the Tianhe-2 Supercomputer.

[1] A. Narayan, A. Cano, A. V. Balatsky, and N. A. Spaldin, Multiferroic quantum criticality, Nat. Mater. **18**, 223 (2019).

[2] C. Wang, L. You, D. Cobden, and J. Wang, Towards two-dimensional van der Waals ferroelectrics, Nat. Mater. **22**, 542 (2023).

[3] A. G. Ricciardulli, S. Yang, J. H. Smet, and M. Saliba, Emerging perovskite monolayers, Nat. Mater. **20**, 1325 (2021).

[4] N. A. Spaldin and R. Ramesh, Advances in magnetoelectric multiferroics, Nat. Mater. **18**, 203 (2019).

[5] X. Wang, Y. Chai, L. Zhou, H. Cao, C.-D. Cruz, J. Yang, J. Dai, Y. Yin, Z. Yuan, S. Zhang *et al.*, Observation of magnetoelectric multiferroicity in a cubic perovskite system: $LaMn_3Cr_4O_{12}$, Phys. Rev. Lett. **115**, 087601 (2015).

[6] W. Li, Z. Wang, F. Deschler, S. Gao, R. H. Friend, and A. K. Cheetham, Chemically diverse and multifunctional hybrid organic–inorganic perovskites, Nat. Rev. Mater. **2**, 16099 (2017).

[7] H. Schmid, Multi-ferroic magnetoelectrics, Ferroelectrics **162**, 317 (1994).

[8] Y. Zhu, J. Xia, S. Wu, K. Sun, Y. Yang, Y. Zhao, H. W. Kan, Y. Zhang, L. Wang, H. Wang *et al.*, Crystal growth engineering and origin of the weak ferromagnetism in antiferromagnetic matrix of orthochromates from t-e orbital hybridization, Iscience **25**, 104111 (2022).

[9] J.-S. Zhou, J. A. Alonso, V. Pomjakushin, J. B. Goodenough, Y. Ren, J.-Q. Yan, and J.-G. Cheng, Intrinsic structural distortion and superexchange interaction in the orthorhombic rare-earth perovskites $R$$CrO_3$, Phys. Rev. B **81**, 214115 (2010).

[10] J.-S. Zhou, J. A. Alonso, A. Muoñz, M. T. Fernández-Díaz, and J. B. Goodenough, Magnetic structure of $LaCrO_3$ perovskite under high pressure from *in situ* neutron diffraction, Phys. Rev. Lett. **106**, 057201 (2011).

[11] E. J. Moon, Q. He, S. Ghosh, B. J. Kirby, S. T. Pantelides, A. Y. Borisevich, and S. J. May, Structural "δ doping" to control local magnetization in isovalent oxide heterostructures, Phys. Rev. Lett. **119**, 197204 (2017).

[12] J. B. Goodenough, Theory of the role of covalence in the perovskite-type manganites [La, M(II)]MnO_3, Phys. Rev. **100**, 564 (1955).

[13] J. B. Goodenough, An interpretation of the magnetic properties of the perovskite-type mixed crystals $La_{1-x}Sr_xCoO_{3-\lambda}$, J. Phys. Chem. Solids **6**, 287 (1958).

[14] J. Kanamori, Superexchange interaction and symmetry properties of electron orbitals, J. Phys. Chem. Solids **10**, 87 (1959).

[15] A. E. Thuijs, X.-G. Li, Y.-P. Wang, K. A. Abboud, X.-G. Zhang, H.-P. Cheng, and G. Christou, Molecular analogue of the perovskite repeating unit and evidence for direct Mn^{III}-Ce_{IV}-Mn^{III} exchange coupling pathway, Nat. Commun. **8**, 500 (2017).

[16] M. Wang, T. Wang, M. Yuan, Q. Zhang, S. Liu, J. Shuai, and X.-G. Li, Molecular analog of perovskite ferrites: First-principles studies of electronic and magnetic properties, Phys. Rev. B **108**, 184421 (2023).

[17] Y.-P. Wang, X.-G. Li, X.-G. Zhang, G. Christou, and H.-P. Cheng, Cation substitution effect on a molecular analogue of perovskite manganites, J. Phys. Chem. C **121**, 10893 (2017).

[18] W. Kohn and L. J. Sham, Self-consistent equations including exchange and correlation effects, Phys. Rev. **140**, A1133 (1965).

[19] J. P. Perdew, K. Burke, and M. Ernzerhof, Generalized gradient approximation made simple, Phys. Rev. Lett. **77**, 3865 (1996).

[20] G. Kresse and J. Furthmüller, Efficiency of *ab-initio* total energy calculations for metals and semiconductors using a plane-wave basis set, Comput. Mater. Sci. **6**, 15 (1996).

[21] G. Kresse and J. Furthmüller, Efficient iterative schemes for *ab initio* total-energy calculations using a plane-wave basis set, Phys. Rev. B **54**, 11169 (1996).

[22] P. E. Blöchl, Projector augmented-wave method, Phys. Rev. B **50**, 17953 (1994).

[23] G. Kresse and D. Joubert, From ultrasoft pseudopotentials to the projector augmented-wave method, Phys. Rev. B **59**, 1758 (1999).

[24] C. Loschen, J. Carrasco, K. M. Neyman, and F. Illas, First-principles LDA+U and GGA+U study of cerium oxides: Dependence on the effective U parameter, Phys. Rev. B **75**, 035115 (2007).

[25] A. A. Mostofi, J. R. Yates, Y.-S. Lee, I. Souza, D. Vanderbilt, and N. Marzari, wannier90: A tool for obtaining maximally-

localised Wannier functions, Comput. Phys. Commun. **178**, 685 (2008).

[26] J. T. Zhang, C. Ji, J. L. Wang, W. S. Xia, X. M. Lu, and J. S. Zhu, Stabilization of E-type magnetic order caused by epitaxial strain in perovskite manganites, Phys. Rev. B **97**, 085124 (2018).

[27] A. O. Shorikov, A. V. Lukoyanov, M. A. Korotin, and V. I. Anisimov, Magnetic state and electronic structure of the δ and α phases of metallic Pu and its compounds, Phys. Rev. B **72**, 024458 (2005).

[28] I. Shein, K. Shein, V. Kozhevnikov, and A. Ivanovskii, Band structure and the magnetic and elastic properties of $SrFeO_3$ and $LaFeO_3$ perovskites, Phys. Solid State **47**, 2082 (2005).

[29] See Supplemental Material at http://link.aps.org/supplemental/10.1103/PhysRevB.110.L020409 for different magnetic ordering for Ce_3Cr_8; detailed information of the t-e hybridization model; total energy, J_2 and J_0 under different Cr $3d$ orbital U values; hopping terms in Ce_3Cr_8 and $[La_3Cr_8]^{-1}$; Wannier orbitals' difference between Ce_3Cr_8 and $[La_3Cr_8]^{-1}$; PDOS in different U values of Ce(La) $4f$ orbitals; and Ce^{III}-O-Cr^{III} exchange interactions in Ce_3Cr_8. The Supplemental Material also contains Ref. [30].

[30] K. Lendi, Extension of the Slater-Koster tables for tight-binding calculations to f electrons, Phys. Rev. B **9**, 2433 (1974).

[31] A. Abbad, W. Benstaali, H. Bentounes, S. Bentata, and Y. Benmalem, Search for half-metallic ferromagnetism in orthorhombic Ce(Fe/Cr)O3 perovskites, Solid State Commun. **228**, 36 (2016).

[32] L. Noodleman, Valence bond description of antiferromagnetic coupling in transition metal dimers, J. Chem. Phys. **74**, 5737 (1981).

[33] L. Noodleman and E. R. Davidson, Ligand spin polarization and antiferromagnetic coupling in transition metal dimers, Chem. Phys. **109**, 131 (1986).

[34] L. Noodleman, C. Peng, D. Case, and J.-M. Mouesca, Orbital interactions, electron delocalization and spin coupling in iron-sulfur clusters, Coord. Chem. Rev. **144**, 199 (1995).

[35] K. Yamaguchi, T. Tsunekawa, Y. Toyoda, and T. Fueno, Ab initio molecular orbital calculations of effective exchange integrals between transition metal ions, Chem. Phys. Lett. **143**, 371 (1988).

[36] K. Yamaguchi, T. Fueno, N. Ueyama, A. Nakamura, and M. Ozaki, Antiferromagnetic spin couplings between iron ions in iron–sulfur clusters. A localized picture by the spin vector model, Chem. Phys. Lett. **164**, 210 (1989).

[37] G. Singh, S. Gamboa, M. Orio, D. A. Pantazis, and M. Roemelt, Magnetic exchange coupling in Cu dimers studied with modern multireference methods and broken-symmetry coupled cluster theory, Theor. Chem. Acc. **140**, 139 (2021).

[38] R. Sessoli and A. K. Powell, Strategies towards single molecule magnets based on lanthanide ions, Coord. Chem. Rev. **253**, 2328 (2009).

[39] J. C. Slater and G. F. Koster, Simplified LCAO method for the periodic potential problem, Phys. Rev. **94**, 1498 (1954).

[40] K. Liu, Y. Hou, X. Gong, and H. Xiang, Orbital delocalization and enhancement of magnetic interactions in perovskite oxyhydrides, Sci. Rep. **6**, 19653 (2016).

[41] P. W. Anderson, New approach to the theory of superexchange interactions, Phys. Rev. **115**, 2 (1959).

[42] X.-G. Li, X.-G. Zhang, and H.-P. Cheng, Conformational electroresistance and hysteresis in nanoclusters, Nano Lett. **14**, 4476 (2014).